NANO LETTERS

Letter

pubs.acs.org/NanoLett

Crab Shells as Sustainable Templates from Nature for Nanostructured Battery Electrodes

Hongbin Yao,[†] Guangyuan Zheng,[‡] Weiyang Li,[†] Matthew T. McDowell,[†] Zhiwei Seh,[†] Nian Liu,[‡] Zhenda Lu,[†] and Yi Cui*[,†,§]

[†]Department of Materials Science and Engineering and [‡]Department of Chemical Engineering, Stanford University, Stanford, California 94305, United States

[§]Stanford Institute for Materials and Energy Sciences, SLAC National Accelerator Laboratory, 2575 Sand Hill Road, Menlo Park, California 94025, United States

Supporting Information

ABSTRACT: Rational nanostructure design has been a promising route to address critical materials issues for enabling next-generation high capacity lithium ion batteries for portable electronics, vehicle electrification, and grid-scale storage. However, synthesis of functional nanostructures often involves expensive starting materials and elaborate processing, both of which present a challenge for successful implementation in low-cost applications. In seeking a sustainable and cost-effective route to prepare nanostructured battery electrode materials, we are inspired by the diversity of natural materials. Here, we show that crab shells with the unique Bouligand structure consisting of highly mineralized chitin-protein fibers can be used as biotemplates to fabricate hollow carbon nanofibers; these fibers can then be used to encapsulate sulfur and silicon to form cathodes and anodes for Li-ion batteries. The resulting nanostructured electrodes show high specific capacities (1230 mAh/g for sulfur and 3060 mAh/g for silicon) and excellent cycling performance (up to 200 cycles with 60% and 95% capacity retention, respectively). Since crab shells are readily available due to the 0.5 million tons produced annually as a byproduct of crab consumption, their use as a sustainable and low-cost nanotemplate represents an exciting direction for nanostructured battery materials.

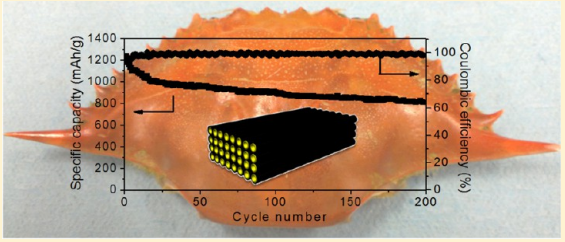

KEYWORDS: *Battery, biotemplates, crab shell, nanostructure electrodes, sulfur, silicon*

High capacity Li-ion battery electrode materials such as Si, Sn, SnO_2, S, and O_2 have attracted great attention due their potential to increase Li-ion battery energy density. For example, silicon anodes[1] and sulfur cathodes[2] offer the very high theoretical specific capacity values of 4200 and 1673 mAh/g, respectively. The theoretical specific energy of full cells consisting of silicon and sulfur electrodes is four times that of existing $LiCoO_2$/graphite batteries.[3−5] However, lithium reacts with these materials through different mechanisms than traditional intercalation-based chemistries, resulting in many new fundamental and applied challenges,[6] including significant morphological/structural changes during battery cycling,[2,7−10] mechanical stress evolution and fracture,[1,11] and instability of the solid electrolyte interface (SEI) on the anode.[12] In the case of lithium−sulfur batteries, additional challenges include the insulating nature of sulfur and lithium sulfide,[13] the dissolution of intermediate lithium polysulfide species,[14−17] and the internal redox shuttle of polysulfide.[14]

Nanoscale materials design for advanced battery electrodes has been shown to be one of the most effective ways to address these issues.[3,12,15,18−29] Many advanced nanosynthesis methods[12,18,22,25,27,28] have been developed to fabricate rationally designed nanostructures, among which nanotemplating is a powerful technique. For instance, electrospun polymer nanofibers were used as a sacrificial template to fabricate double-walled silicon nanotubes that could accommodate lithiation-induced volume changes while maintaining a stable SEI during cycling.[12] In another example, silica coatings on silicon nanoparticles were used as a sacrificial layer for synthesizing silicon/carbon yolk-shell nanostructures to promote stable and self-limiting SEI growth.[21] For sulfur batteries, mesoporous carbon has been used to overcome the insulating nature of sulfur and to trap polysulfides in the cathode architecture; these mesoporous carbon particles are synthesized from mesoporous silica sacrificial templates.[15,20] Anodized aluminum oxide (AAO) templates have been used to fabricate silicon nanotubes for direct use as anodes[25] and also hollow carbon nanofiber/sulfur composites for a cathode material.[22] Finally, hollow SnO_2 spheres were used as a hard template to synthesize double-shelled hollow carbon spheres for sulfur cathode applications.[24] While all of these demonstrations have shown the advantages of nanostructuring the electrode for better battery perform-

Received: May 11, 2013
Revised: June 6, 2013

   dx.doi.org/10.1021/nl401729r | *Nano Lett.* XXXX, XXX, XXX−XXX

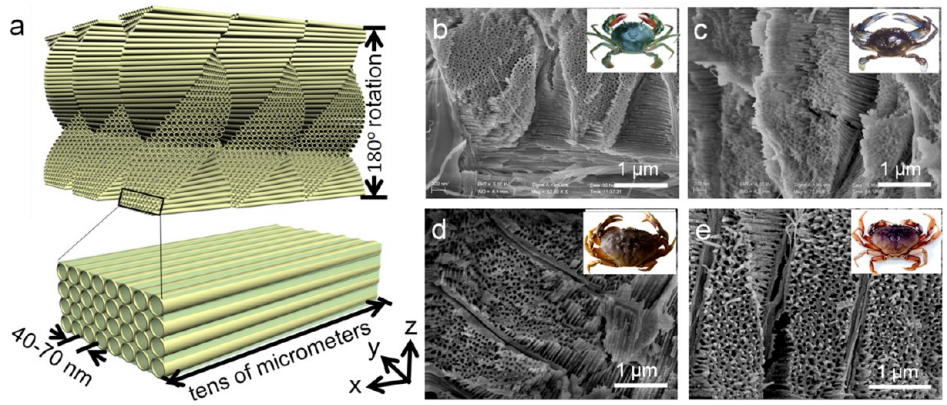

Figure 1. Structural model and SEM images of crab shell templates. (a) Structural model of twisted plywood nanochannel arrays in crab shell templates showing the hollow channels created by removing organic nanofibers in crab shells. The hollow channels are arranged parallel to each other to form horizontal planes stacked in a helicoid fashion, creating a twisted plywood structure. (b–e) SEM images of the biotemplates from a Chinese hairy crab shell, a blue crab, a stone crab, and a Dungeness crab, respectively, demonstrating the universal nature of the nanochannel arrays in crab shell templates.

ance,[4,12,15,22,25] low-cost, scalable, and sustainable nanostructured templates are highly desirable.

Diverse biomaterials with hierarchical structures[30–33] created by nature have provided a number of sustainable templates for synthesizing functional nanostructured materials for various applications such as photonic crystals, magnets, and sensors.[31,33–37] However, it is not yet clear whether sustainable biotemplates exist for high-performance battery applications. Herein, we show that crab shells are excellent biotemplates for the fabrication of nanostructured electrode materials with excellent performance.

Crab shells are a sustainable natural resource since 1.5 million tons of crabs are consumed every year, generating about 0.5 million tons of crab shells as waste. This is much more than current Li-ion battery electrode material production (tens of thousands of tons including both anodes and cathodes). Crab exoskeletons are natural composites consisting of highly mineralized chitin–protein nanofibers with an average diameter of 60 nm arranged in a twisted plywood or Bouligand pattern with bioceramic $CaCO_3$.[38–41] Using simple thermal calcination in air, the chitin-protein organic components in the exoskeletons can be removed to form pure $CaCO_3$ frameworks containing twisted hollow channels with ~60 nm inner diameter, which is similar to the diameter found in commonly used AAO templates. As illustrated in Figure 1a, the hollow nanochannels created by removing the organic nanofibers are arranged parallel to each other, forming horizontal planes. These planes are stacked in a helicoid fashion, creating a twisted plywood structure. A stack of layers completing a 180° rotation is referred to as a Bouligand structure; this structure is repeated in the *z*-direction, forming the whole crab shell template.

To demonstrate the universal presence of these nanochannel array structures in crab shells, we used scanning electron microscopy (SEM) to study the microstructures of the templates from four different common crab varieties (Chinese hairy crab, blue crab, stone crab, and Dungeness crab). As shown in Figure 1b–e, all of these crab shell templates contain nanochannel arrays with uniform diameters. The statistical distribution of nanochannel diameter in the four crab shell templates is shown in Supporting Information, Figures S1–4. There is very little difference in the channel diameter for different types of crabs; they all have diameters in the range of 40–70 nm. The nanochannels are arranged hexagonally with significant disorder, and the center-to-center spacing of the nanochannels is 90–150 nm. It is difficult to determine the length of the individual channels but it is most likely tens of micrometers. Based on understanding from previous nanostructure design for advanced lithium ion rechargeable batteries,[12,15,22,25] we believed that the crab shell nanotemplates present the following interesting features: (1) The high surface area of the inner surface is important for depositing active materials to retain high activity of electrode; (2) The empty space inside the nanochannel arrays can accommodate the volume change of the active materials during charge/discharge processes; (3) One-dimensional hollow structures are efficient in confining active materials to reduce their contact with the electrolyte or their diffusion into the electrolyte; (4) Nanowire-like materials templated from nanochannel arrays can facilitate fast lithium ion transport through the side wall between the active material and the electrolyte to achieve high capacity at a high power rate; and finally, (5) The crab shell template is only composed of $CaCO_3$, which can easily be etched using dilute HCl solution, a relatively environmentally benign route as compared to the HF acid used for silica template etching.[15,20,21]

Given the similarity of the nanochannels in the four different types of crab shells, we chose the stone crab shells as the main biotemplates for our work due to their wide availability. As shown in Figure 2a, the thickness and horizontal width of a stone crab shell can reach 0.5 mm and 10.8 cm, respectively, and the whole crab shell is composed of layers of packed chitin–protein nanofibers parallel to the horizontal plane of shell. Through simple thermal decomposition of the chitin–protein nanofibers in the stone crab shell, a $CaCO_3$ template consisting of nanoscale channels with a twisted plywood arrangement was obtained (Figure 2b). Usually, one piece of crab shell (15 g) can yield about 8 g of nanostructured $CaCO_3$ (inset in Figure 2b). The nanoscale channels in the $CaCO_3$ templates obtained from the stone crab shells have high packing density and uniform pore sizes, as shown in Figure 2c. The diameter distribution of these nanoscale channels (Figure 2d) indicates an average diameter of about 70 nm.

The procedure for fabricating sulfur and silicon battery electrodes from these templates is shown in Figure 2e (see Supporting Information for more experimental details). First, a thin layer of carbon was coated on the whole surface of the

dx.doi.org/10.1021/nl401729r | *Nano Lett.* XXXX, XXX, XXX–XXX

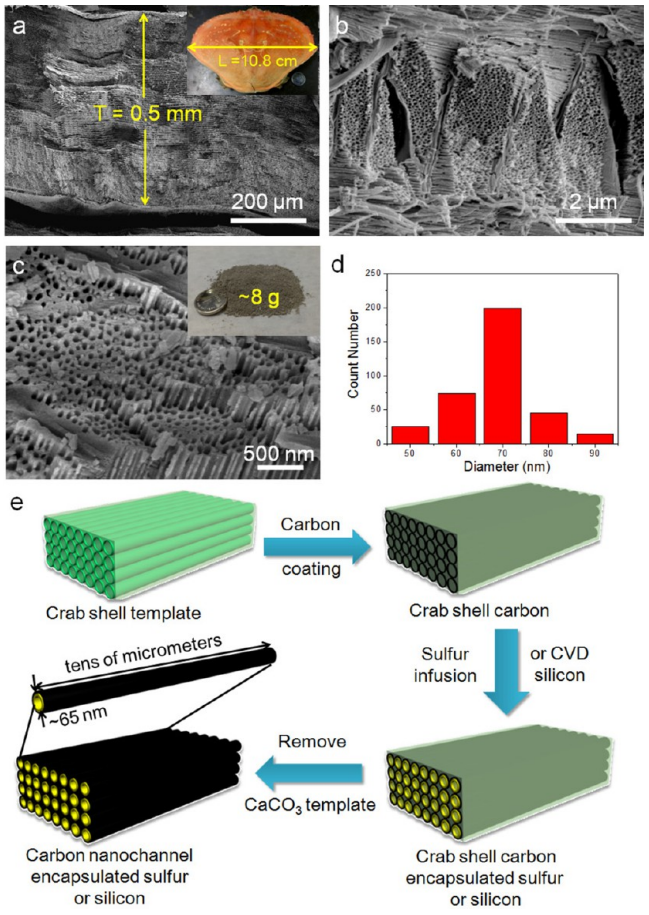

Figure 2. Nanostructure of stone crab shell template and schematic illustration of the fabrication procedure of electrode materials. (a–c) SEM images of the cross section of a stone crab shell, a stone crab shell template, and the powder of the stone crab shell template, respectively. The inset in a shows that the length of the stone crab shell is 10.8 cm, and the inset in c shows that about 8 g of powder was produced from one piece of stone crab shell. (d) Statistics of the diameter distribution of the nanoscale channels in stone crab shell biotemplates. (e) Schematic illustration of the fabrication procedure for hollow carbon nanofiber arrays encapsulating sulfur or silicon electrode materials based on stone crab shell templates.

$CaCO_3$ framework. Next, the battery active electrode materials were loaded into the nanochannels: sulfur was introduced by thermal infusion, while silicon was deposited by chemical vapor deposition (CVD). After dissolving away the $CaCO_3$ framework in 2 M HCl solution, hollow carbon nanofiber arrays encapsulating either sulfur or silicon were obtained. As a result of this preparation process, the sulfur and silicon active materials are only coated on the interior of the hollow carbon fiber arrays. As shown in previous studies,[12,21,22] coating materials onto interior walls of hollow structures is important for reducing deleterious interactions of the active material with the electrolyte. The hollow carbon nanofiber inner diameter is about 65 nm, while the length is up to tens of micrometers. The active battery material (sulfur or silicon) is effectively confined in these high aspect-ratio hollow carbon nanofibers to limit its contact with the electrolyte. The hollow nanostructures will also provide sufficient space for the volume expansion of sulfur/silicon during the discharge/charge processes. In addition, the thin walls of the hollow carbon nanofibers allow rapid lithium ion transport from the electrolyte to sulfur/silicon, and the one-dimensional structure of the carbon wall can enable fast electron transfer from the current collector to the active materials.

During the synthesis process shown in Figure 2e, it is important that the coating method produces a conformal and uniform carbon layer onto the $CaCO_3$ without destroying the nanostructured template. We have tried three methods and have identified that a dopamine self-polymerization method works the best. A dopamine aqueous solution at pH 8.5 in the presence of oxygen was used to coat $CaCO_3$, where the dopamine self-polymerized and formed a uniform polymer coating on the surface of the $CaCO_3$ framework. As shown in Figure 3a, after dopamine self-polymerization, the surface of the

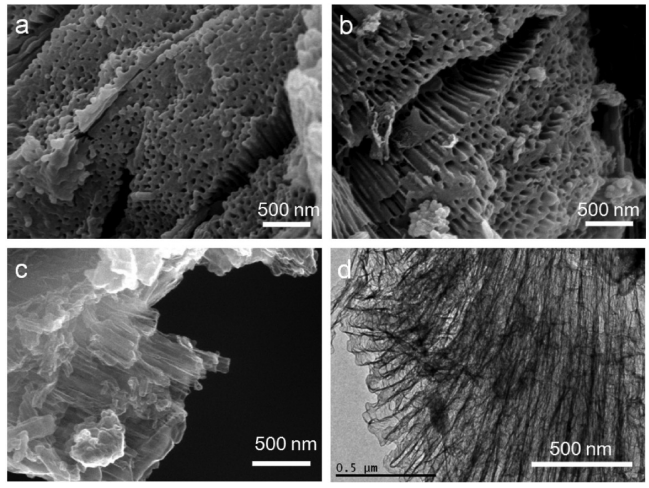

Figure 3. SEM and TEM characterization to show the preservation of nanochannel arrays during the carbon coating process. (a–c) SEM images of polydopamine-coated crab shell template, carbon-coated crab shell template, and carbon nanochannel arrays after removing the $CaCO_3$ framework, respectively. (d) TEM image of carbon nanochannel arrays after removing the $CaCO_3$ framework.

$CaCO_3$ template became smooth with decreased inner diameter of the nanochannels, but the hollow nanochannel structures still remained. The polydopamine coating was easily transformed into a carbon coating on the surface of the $CaCO_3$ template via an annealing process at 800 °C under N_2 atmosphere.[21,42] Figure 3b shows an SEM image of the carbon-coated $CaCO_3$, revealing that the carbon layer was uniformly coated on the template and that the nanostructure of the crab shell template was preserved after carbonization. After dissolving the $CaCO_3$ framework, both SEM and TEM images (Figure 3c and d) confirmed that well-defined hollow carbon nanofiber arrays were obtained. Therefore, the hollow nanochannels in crab shell biotemplates were transformed into conductive hollow carbon nanofibers. The polydopamine coating method is more effective for obtaining the desired structure from crab shell templates than previously reported chemical vapor deposition (CVD) carbon coating[22] or polymer solution infusion methods.[43] In our tests, CVD carbon coating produced collapsed carbon nanocages, resulted from the instability of $CaCO_3$ under CVD conditions (see Figure S5, SI). Although the regular polymer solution infusion did not destroy the nanochannel structures in $CaCO_3$ templates, the random shrinkage of polymer during drying and carbonization processes led to the formation of porous carbon nanofibers with fractured walls (see Figure S6, SI).

dx.doi.org/10.1021/nl401729r | Nano Lett. XXXX, XXX, XXX–XXX

The carbon-coated hollow nanofibers are a good host for sulfur or silicon loading. To demonstrate the usefulness of the biotemplated hollow carbon fibers, we first study sulfur cathodes. The SEM image in Figure 4a clearly shows the uniform nanochannel array structures of the as-prepared carbon/sulfur composite in which no bulk sulfur particles were observed, indicating the full incorporation of sulfur into the hollow carbon nanofibers. Further evidence of the filling of carbon nanochannels with sulfur was provided by TEM. As shown in Figure 4b, the sulfur was loaded into hollow carbon nanofibers. The darker area in the TEM image denotes the location of sulfur, as it is heavier and thicker than carbon. Energy dispersive X-ray spectroscopy (EDX) analysis (Figure 4c) demonstrated the presence of sulfur in the carbon nanochannels without other impurities. Thermogravimetric analysis (TGA) of the carbon/sulfur composite under argon flow showed a weight loss of about 65% from 200 to 300 °C (see Figure S7, SI), which corresponds to the weight percent of sulfur loading in the composite.

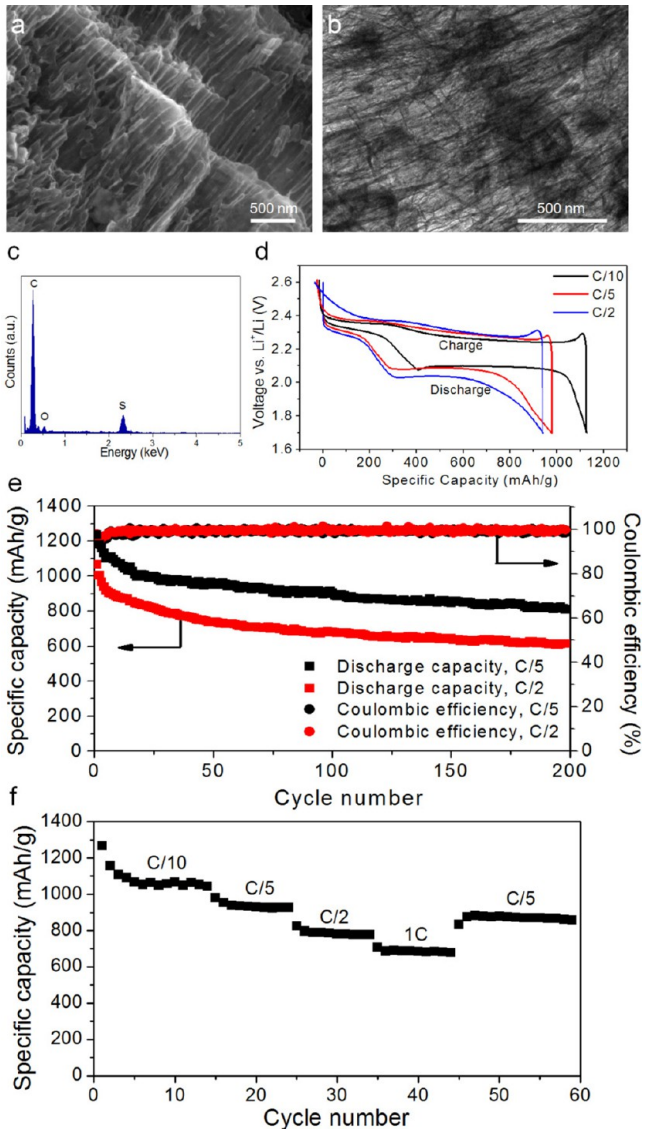

Figure 4. Nanostructures and electrochemical performance of sulfur encapsulated by crab shell-templated carbon as Li-ion battery electrode. (a and b) SEM and TEM images of sulfur encapsulated by crab shell-templated carbon showing nanochannel array structures. (c) EDX spectrum indicating the presence of sulfur and carbon without other impurities. (d) Typical discharge/charge voltage profiles of the sulfur electrode at *C*/10, *C*/5, and *C*/2 rates. (e) Capacity and Coulombic efficiency at *C*/5 and *C*/2 versus cycle number. (f) Rate capabilities on discharge of the crab shell-templated sulfur electrode.

Coin cells with Li metal as the counter/reference electrode were fabricated to test the battery performance. The typical mass loading of sulfur in the electrode was 0.8 mg/cm^2, and the specific capacities were calculated based on the sulfur mass only. Typical discharge/charge voltage profiles of the carbon/sulfur composites at different current rates (*C*/10, *C*/5, and *C*/2, where 1*C* = 1673 mA/g) are shown in Figure 4d. All discharge voltage profiles at *C*/10, *C*/5, and *C*/2 rates display the typical two-plateau behavior of S cathodes. The first plateau corresponds to the formation of long chain polysulfides (Li_2S_x, $4 \leq x \leq 8$) from element sulfur at 2.0−2.4 V. The second plateau around 2.0 V is attributed to the conversion of polysulfides to Li_2S_2 and then to Li_2S. The flat second plateau suggests a uniform deposition of solid Li_2S_2 or Li_2S on carbon surface with little kinetic barrier. The cycling performance is shown in Figure 4e. At a *C*/5 rate, an initial capacity of 1230 mAh/g was obtained, indicating 73% sulfur utilization during the first discharge process. After 100 cycles of reversible discharge/charge at a *C*/5 rate, the capacity of the cell was 880 mAh/g; this results in capacity retention of 71% after 100 cycles, which is better than that of our previously reported graphene-wrapped sulfur and AAO template-fabricated hollow carbon nanofiber encapsulated sulfur cathodes.[22,44] A reversible capacity of around 810 mAh/g was still retained after 200 cycles, corresponding to a capacity retention of 65%. The average Coulombic efficiency of the cell at *C*/5 is around 99.2%. The cell also exhibits good cycling performance at a *C*/2 discharge/charge rate with a reversible capacity of around 610 mAh/g and average Coulombic efficiency of 99.5% for 200 cycles. Cycling rates up to 1*C* are shown in Figure 4f, demonstrating a good rate capability. The discharge capacity steadily changed as the current rate increased from *C*/10 to 1*C*, with reversible capacities of 1050, 920, 786, and 690 mAh/g at *C*/10, *C*/5, *C*/2, and 1*C*, respectively. When the current rate was reduced back to *C*/5, the cell recovered to nearly the original *C*/5 capacity level, indicating robustness and stability of the cathode structure. These results show that the performance of crab shell-templated carbon-encapsulated sulfur is comparable to or even better than that of previously reported carbon/sulfur composite cathodes derived from AAO templating carbon,[22] mesoporous carbon,[15] porous carbon spheres,[23] and double-shell hollow carbon spheres.[24]

To extend the biotemplated hollow carbon nanofiber architecture to other battery materials, we have developed Si anodes based on this structure. Figure 5a shows an SEM image of the as-synthesized crab shell-templated carbon/silicon composite, demonstrating that the silicon was deposited on the surface of the hollow carbon nanofibers. The TEM image in Figure 5b further shows the nanochannel array structures of our synthesized carbon/silicon composites. EDX (Figure 5c) confirms that the obtained composite contains carbon and silicon. TGA (Figure S8) carried out under mixed atmosphere of Ar and O_2 (V_{Ar}:V_{O_2} = 4:1) indicates that the content of silicon in the as-synthesized composite is around 92 wt %. In the TGA curve, the first weight loss before 500 °C is caused by the oxidation of carbon to become gaseous CO_2, and the later

dx.doi.org/10.1021/nl401729r | *Nano Lett.* XXXX, XXX, XXX−XXX

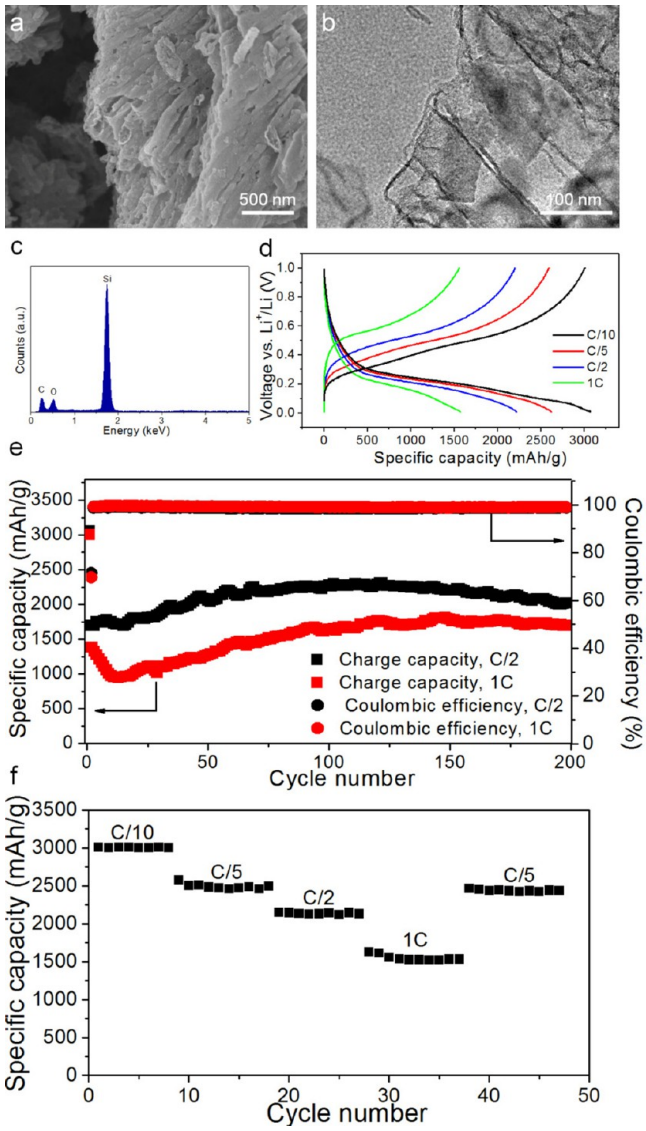

Figure 5. Nanostructures and electrochemical performance of silicon encapsulated in crab shell-templated carbon for Li-ion battery electrodes. (a and b) SEM and TEM images showing the nanochannel array structure. (c) EDX spectrum indicating the presence of carbon and silicon. (d) Typical discharge/charge voltage profiles at *C*/10, *C*/5, *C*/2, and 1*C* rates. (e) Reversible capacity and Coulombic efficiency at *C*/2 and 1*C* versus cycle number. The cells were activated with a slower rate on the first cycle (*C*/10). (f) Rate capabilities of the electrode.

weight increase after 500 °C is attributed to the oxidation of silicon.

The electrochemical performance of the crab shell-templated carbon/silicon composite was evaluated in coin cells with a metallic Li counter/reference electrode. The specific capacities were calculated based on the silicon mass only, and the mass loading of silicon on the electrode was around 0.1 mg/cm^2. Typical discharge/charge voltage profiles are shown in Figure 5d, indicating that the specific capacities of cells at *C*/10, *C*/5, *C*/2, and 1*C* are 3060, 2620, 2210, and 1580 mAh/g, respectively. These specific capacities at different current rates are comparable to that of silicon anodes generated from AAO and electrospun nanofiber templates.[12,25] The crab shell-templated carbon/silicon composite anodes also displayed excellent cycling performance. As shown in Figure 5e, the reversible specific capacity of our fabricated cells can be maintained around 2010 mAh/g and 1690 mAh/g without any capacity decay after 200 cycles at *C*/2 and 1*C*, respectively. The capacity increase during the first part of cycling is due to a delayed activation process resulting from the insufficient lithiation during the initial cycle at *C*/10. This is related to electrolyte wetting and an increase in electrical and ionic conductivity after lithium insertion. The excellent cycling performance of the cells based on crab shell-templated carbon/silicon composites is attributed to the void space in the carbon nanochannels that can accommodate the volume change of silicon during discharge/charge processes and also the efficient encapsulation of silicon in the hollow carbon nanofiber arrays to avoid continual formation of SEI. The Coulombic efficiencies of our cells over 200 cycles are ~98.6% at *C*/2 and ~98.9% at 1*C*. The cell also demonstrates good rate capability. As shown in Figure 5f, the capacity of the cell steadily varied with the increase of current rate from *C*/10 to 1*C*, and a stable reversible capacity of 1520 mAh/g is obtained at a 1*C* rate. The capacity of the cell recovered well when the current rate increased back to *C*/5, indicating the stability of crab shell-templated carbon/silicon anode materials.

Compared to previously reported nanostructured carbon materials, our crab shell-templated hollow carbon nanofiber arrays show high performance (high capacity and good cycling stability) for both sulfur cathodes and silicon anodes. The electrochemical performance is comparable to or even better than that of previously reported nanostructured electrodes such as AAO-templated carbon/sulfur cathodes[22] and silicon anodes,[25] mesoporous carbon/sulfur cathodes,[15] porous carbon sphere/sulfur cathodes,[23] double-walled silicon nanotube anodes,[12] and yolk-shell nanostructured silicon anodes.[21] The high performance of crab shell-templated carbon is enabled by the mitigation of polysulfide dissolution and the avoidance of continual growth of SEI on silicon. Most importantly, the natural and sustainable crab shells provide a cost-effective and environmentally friendly source of nanostructured electrode material.

In summary, we have demonstrated the successful use of crab shell nanochannel templates to construct hollow nanofiber electrodes for advanced rechargeable lithium ion batteries with high specific capacity and long cycle life. This biotemplating concept will open a new avenue for producing nanostructured electrode materials from low-cost sustainable sources.

■ ASSOCIATED CONTENT

Supporting Information

Experimental section, SEM images of crab shell templates, statistical distribution of inner diameter of crab shell nanochannels, TEM images carbon templates, and TGA data of sulfur cathodes and silicon anode. This material is available free of charge via the Internet at http://pubs.acs.org.

■ AUTHOR INFORMATION

Corresponding Author

*E-mail: yicui@stanford.edu.

Author Contributions

H.Y. and Y.C. conceived the idea. H.Y. and N.L. carried out materials synthesis and electrochemical tests. H.Y., G.Z., and W.L. performed materials characterization. Z.S. and Z.L. contributed to the discussion of the results. H.Y. and Y.C.

dx.doi.org/10.1021/nl401729r | *Nano Lett.* XXXX, XXX, XXX−XXX

cowrote the paper. All of the authors commented on and revised the manuscript.

Notes

The authors declare no competing financial interest.

■ ACKNOWLEDGMENTS

This work was supported by the Assistant Secretary for Energy Efficiency and Renewable Energy, Office of Vehicle Technologies of the U.S. Department of Energy under Contract No. DE-AC02-05CH11231, Subcontract No. 6951379 under the Batteries for Advanced Transportation Technologies (BATT) Program.

■ REFERENCES

(1) Boukamp, B. A.; Lesh, G. C.; Huggins, R. A. *J. Electrochem. Soc.* **1981**, *128*, 725−729.
(2) Shim, J.; Striebel, K. A.; Cairns, E. J. *J. Electrochem. Soc.* **2002**, *149*, A1321−A1325.
(3) Yang, Y.; McDowell, M. T.; Jackson, A.; Cha, J. J.; Hong, S. S.; Cui, Y. *Nano Lett.* **2010**, *10*, 1486−1491.
(4) Liu, N.; Hu, L.; McDowell, M. T.; Jackson, A.; Cui, Y. *ACS Nano* **2011**, *5*, 6487−6493.
(5) Elazari, R.; Salitra, G.; Gershinsky, G.; Garsuch, A.; Panchenko, A.; Aurbach, D. *Electrochem. Commun.* **2012**, *14*, 21−24.
(6) Tarascon, J. M.; Armand, M. *Nature* **2001**, *414*, 359−367.
(7) Kasavajjula, U.; Wang, C.; Appleby, A. J. *J. Power Sources* **2007**, *163*, 1003−1039.
(8) Beaulieu, L. Y.; Eberman, K. W.; Turner, R. L.; Krause, L. J.; Dahn, J. R. *Electrochem. Solid-State Lett.* **2001**, *4*, A137−A140.
(9) Cheon, S.-E.; Ko, K.-S.; Cho, J.-H.; Kim, S.-W.; Chin, E.-Y.; Kim, H.-T. *J. Electrochem. Soc.* **2003**, *150*, A796−A799.
(10) Chan, C. K.; Ruffo, R.; Hong, S. S.; Huggins, R. A.; Cui, Y. *J. Power Sources* **2009**, *189*, 34−39.
(11) Cheon, S.-E.; Ko, K.-S.; Cho, J.-H.; Kim, S.-W.; Chin, E.-Y.; Kim, H.-T. *J. Electrochem. Soc.* **2003**, *150*, A800−A805.
(12) Wu, H.; Chan, G.; Choi, J. W.; Ryu, I.; Yao, Y.; McDowell, M. T.; Lee, S. W.; Jackson, A.; Yang, Y.; Hu, L.; Cui, Y. *Nat. Nanotechnol.* **2012**, *7*, 310−315.
(13) Barchasz, C.; Leprêtre, J.-C.; Alloin, F.; Patoux, S. *J. Power Sources* **2012**, *199*, 322−330.
(14) Mikhaylik, Y. V.; Akridge, J. R. *J. Electrochem. Soc.* **2004**, *151*, A1969−A1976.
(15) Ji, X.; Lee, K. T.; Nazar, L. F. *Nat. Mater.* **2009**, *8*, 500−506.
(16) Ji, X.; Nazar, L. F. *J. Mater. Chem.* **2010**, *20*, 9821−9826.
(17) Ji, X.; Evers, S.; Black, R.; Nazar, L. F. *Nat. Commun.* **2011**, *2*, 325.
(18) Chan, C. K.; Peng, H.; Liu, G.; McIlwrath, K.; Zhang, X. F.; Huggins, R. A.; Cui, Y. *Nat. Nanotechnol.* **2008**, *3*, 31−35.
(19) Armand, M.; Tarascon, J. M. *Nature* **2008**, *451*, 652−657.
(20) Liang, C.; Dudney, N. J.; Howe, J. Y. *Chem. Mater.* **2009**, *21*, 4724−4730.
(21) Liu, N.; Wu, H.; McDowell, M. T.; Yao, Y.; Wang, C.; Cui, Y. *Nano Lett.* **2012**, *12*, 3315−3321.
(22) Zheng, G.; Yang, Y.; Cha, J. J.; Hong, S. S.; Cui, Y. *Nano Lett.* **2011**, *11*, 4462−4467.
(23) Jayaprakash, N.; Shen, J.; Moganty, S. S.; Corona, A.; Archer, L. A. *Angew. Chem., Int. Ed.* **2011**, *50*, 5904−5908.
(24) Zhang, C.; Wu, H. B.; Yuan, C.; Guo, Z.; Lou, X. W. *Angew. Chem., Int. Ed.* **2012**, *51*, 9592−9595.
(25) Park, M.-H.; Kim, M. G.; Joo, J.; Kim, K.; Kim, J.; Ahn, S.; Cui, Y.; Cho, J. *Nano Lett.* **2009**, *9*, 3844−3847.
(26) Shi, Y.; Guo, B.; Corr, S. A.; Shi, Q.; Hu, Y.-S.; Heier, K. R.; Chen, L.; Seshadri, R.; Stucky, G. D. *Nano Lett.* **2009**, *9*, 4215−4220.
(27) Jung, D. S.; Hwang, T. H.; Park, S. B.; Choi, J. W. *Nano Lett.* **2013**, *13*, 2092−2097.
(28) Lee, H.; Cho, J. *Nano Lett.* **2007**, *7*, 2638−2641.
(29) Cui, L.-F.; Ruffo, R.; Chan, C. K.; Peng, H.; Cui, Y. *Nano Lett.* **2008**, *9*, 491−495.
(30) Yao, H.-B.; Fang, H.-Y.; Wang, X.-H.; Yu, S.-H. *Chem. Soc. Rev.* **2011**, *40*, 3764−3785.
(31) Sotiropoulou, S.; Sierra-Sastre, Y.; Mark, S. S.; Batt, C. A. *Chem. Mater.* **2008**, *20*, 821−834.
(32) Zhou, H.; Fan, T.; Zhang, D. *ChemSusChem* **2011**, *4*, 1344−1387.
(33) Huebsch, N.; Mooney, D. J. *Nature* **2009**, *462*, 426−432.
(34) Fratzl, P.; Weinkamer, R. *Prog. Mater. Sci.* **2007**, *52*, 1263−1334.
(35) Galusha, J. W.; Jorgensen, M. R.; Bartl, M. H. *Adv. Mater.* **2010**, *22*, 107−110.
(36) Losic, D.; Mitchell, J. G.; Voelcker, N. H. *Adv. Mater.* **2009**, *21*, 2947−2958.
(37) Schnepp, Z.; Yang, W.; Antonietti, M.; Giordano, C. *Angew. Chem., Int. Ed.* **2010**, *49*, 6564−6566.
(38) Bouligand, Y. *Tissue Cell* **1972**, *4*, 189−217.
(39) Roer, R.; Dillaman, R. *Am. Zool.* **1984**, *24*, 893−909.
(40) Giraud-Guille, M.-M. *Curr. Opin. Solid State Mater. Sci.* **1998**, *3*, 221−227.
(41) Chen, P.-Y.; Lin, A. Y.-M.; McKittrick, J.; Meyers, M. A. *Acta Biomater.* **2008**, *4*, 587−596.
(42) Liu, R.; Mahurin, S. M.; Li, C.; Unocic, R. R.; Idrobo, J. C.; Gao, H.; Pennycook, S. J.; Dai, S. *Angew. Chem., Int. Ed.* **2011**, *50*, 6799−6802.
(43) Guo, J.; Xu, Y.; Wang, C. *Nano Lett.* **2011**, *11*, 4288−4294.
(44) Wang, H.; Yang, Y.; Liang, Y.; Robinson, J. T.; Li, Y.; Jackson, A.; Cui, Y.; Dai, H. *Nano Lett.* **2011**, *11*, 2644−2647.